Probing Muonic Forces and Dark Matter at Kaon Factories

Gordan Krnjaic,[1] Gustavo Marques-Tavares,[2, 3] Diego Redigolo,[4, 5, 6] and Kohsaku Tobioka[7, 8]

[1]*Fermi National Accelerator Laboratory, Batavia, IL*
[2]*Maryland Center for Fundamental Physics, Department of Physics,*
University of Maryland, College Park, MD 20742
[3]*Stanford Institute for Theoretical Physics,*
Stanford University, Stanford, CA 94305, USA
[4]*Tel-Aviv University, Tel-Aviv Israel*
[5]*Institute for Advanced Study, Princeton, NJ USA*
[6]*Weizmann Institute of Science, Rehovot Israel*
[7]*Florida State University, Tallahassee, FL USA*
[8]*High Energy Accelerator Research Organization (KEK), Tsukuba Japan*

Rare kaon decays are excellent probes of light, new weakly-coupled particles. If such particles X couple preferentially to muons, they can be produced in $K \to \mu\nu X$ decays. In this letter we evaluate the future sensitivity for this process at NA62 assuming X decays either invisibly or to di-muons. Our main physics target is the parameter space that resolves the $(g-2)_\mu$ anomaly, where X is a gauged $L_\mu - L_\tau$ vector or a muon-philic scalar. The same parameter space can also accommodate dark matter freeze out or reduce the tension between cosmological and local measurements of H_0 if the new force decays to dark matter or neutrinos, respectively. We show that for invisible X decays, a dedicated single muon trigger analysis at NA62 could probe much of the remaining $(g-2)_\mu$ favored parameter space. Alternatively, if X decays to muons, NA62 can perform a di-muon resonance search in $K \to 3\mu\nu$ events and greatly improve existing coverage for this process. Independently of its sensitivity to new particles, we find that NA62 is also sensitive to the Standard Model predicted rate for $K \to 3\mu\nu$, which has never been measured.

I. INTRODUCTION

Light weakly-coupled forces arise in many compelling extensions of the Standard Model (SM) and are the focus of a broad, international experimental effort [1–3]. If such forces couple preferentially to muons, they offer the last viable opportunity to resolve the longstanding $\sim 3.5\,\sigma$ anomaly in $(g-2)_\mu$ [4–6] with new physics below the electroweak scale as originally proposed in [7].[1] Thus, there is strong motivation to improve experimental sensitivity to these interactions.

Independently of this motivation, there is abundant evidence for the existence of dark matter (DM), whose microscopic properties remain elusive despite decades of dedicated searches [9]. One possible explanation for these null results is that DM couples more strongly to the second and third generation. Indeed, there are several consistent, viable, and *predictive* dark forces which mediate DM freeze-out to higher generation particles [10, 11]. Since muonic forces don't couple directly to first generation particles, these DM candidates are difficult to probe with direct detection experiments, but can be efficiently produced at accelerators.

It is well known that light muonic forces can be produced radiatively in rare kaon decays [12–14]. However, there are several timely reasons to revisit this subject:

1. The NA62 experiment [15] is currently producing unprecedented numbers of kaons, and is poised to considerably improve sensitivity to muonic forces.

2. In the next few years, the Fermilab $g-2$ collaboration [16] and the J-PARC $g-2$ experiment [17] will decisively test the $(g-2)_\mu$ anomaly. If this discrepancy is due to new physics, the particles responsible necessarily predict SM deviations in other, complementary muonic systems.

3. Recently there has been great interest in new proposals for dedicated experiments to probe muonic forces [11, 18–21]. To properly assess the merits of these ideas in the long-term, it is essential to know what current and near-term efforts can achieve.

In this letter we show that existing and planned kaon factories, are powerful probes of rare $K \to \mu\nu X$ decays where X is a new vector or scalar particle that couples preferentially to muons. Our main focus are the new physics opportunities of the NA62 experiment at CERN [22], which will produce roughly 10^{13} K^+ in the decay region of the detector.

If X decays invisibly, we find that, with a dedicated single muon trigger, NA62 could have unprecedented sensitivity to $K \to \mu\nu X(X \to \text{invisible})$ processes. Such a search could probe nearly all of the remaining parameter space in which muonic forces reconcile the $(g-2)_\mu$ anomaly. If the invisible decay daughters are DM particles, this also enables X-mediated thermal freeze out [11]; if, instead, these daughters are neutrinos, this parameter space can also ease the $\sim 3.5\sigma$ tension between

---

[1] Light new particles with appreciable couplings to the first generation have been ruled out as possible explanations in simple models, including both visibly and invisibly decaying dark photons (see [3] for a review and [8] for recent discussion).

early and late time measurements of H_0 [23].

If X decays visibly to muons, we find that an NA62 di-muon resonance search in $K \to \mu\nu X(X \to \mu^+\mu^-)$ processes could greatly improve the existing constraints for both scalar and vector muonic forces, thereby covering some of the $(g-2)_\mu$ favored region for $m_K - m_\mu > m_X > 2m_\mu$. The irreducible SM background for this search arises from $K \to 3\mu\nu$ decays which have never been observed before; intriguingly, we find that NA62 can measure this process by reanalyzing already collected data (see [24] for the current best upper bound).

II. VECTOR FORCES

A. Gauged $L_\mu - L_\tau$

A new massive vector boson V gauging a spontaneously broken $L_\mu - L_\tau$ symmetry is a minimal candidate to explain the $(g-2)_\mu$ anomaly. The Lagrangian for this model contains

$$\mathcal{L} \supset \frac{m_V^2}{2}V_\mu V^\mu + V_\mu \left(g_V J_V^\mu + \epsilon e J_{\rm EM}^\mu\right), \quad (1)$$

where g_V is the gauge coupling and m_V is the vector's mass and J_V^μ is the $L_\mu - L_\tau$ current [31]. Loops of taus and muons induce an irreducible kinetic mixing of V_μ with SM photon $\epsilon \simeq g_V/67$ which yields the coupling to the EM current $J_{\rm EM}^\mu$ in Eq. (1). The rest frame partial widths for $V \to f\bar{f}$ are

$$\Gamma_{V \to f\bar{f}} = \frac{\alpha_V m_V}{3}\left(1 + \frac{2m_\mu^2}{m_V^2}\right)\sqrt{1 - \frac{4m_\mu^2}{m_V^2}}, \quad (2)$$

where $f = \mu, \tau$ and $\alpha_V \equiv g_V^2/4\pi$, and the width to neutrino flavor ν_f is $\Gamma_{V \to \nu_f\bar{\nu}_f} = \alpha_V m_V/6$. Decays through the EM current are suppressed by additional factors of $\epsilon^2\alpha/\alpha_V$, so we neglect these here. In all of the parameter space we consider here, V decays promptly within the 65 m decay region at NA62.

For m_V below the weak scale, the existing constraints arise from modifications of neutrino scattering observables and from B-factories. Di-muon production in neutrino trident scattering $\nu N \to \nu N \mu^+\mu^-$ has been measured by the NuTeV [32], CHARM II [26], and CCFR [28] experiments and constrains the rate of additional V mediated contributions to this process. The orange shaded band in Fig. 1 presents the conservative CHARM II bound and the dotted orange curve shows the more constraining CCFR result.[2] Due to the kinetic mixing

---

with the SM photon in Eq. (1), solar neutrinos can scatter with electrons by exchanging t-channel V particles, so this model is constrained by Borexino [21, 34, 35]. The dashed Borexino bound in Fig. 1 assumes only the irreducible contribution to the mixing from tau and muon loops. A comparable bound can be derived from overcooling of white dwarfs from neutrino pair emission from an off-shell V [36, 37]. Finally, for $m_V > 2m_\mu$ the $BABAR$ 4μ search [25] constrains V radiation from final state muons in $e^+e^- \to \mu^+\mu^-V(V \to \mu^+\mu^-)$.

Although our analysis could be extended to arbitrarily low masses, we require $m_V \gtrsim 1$ MeV to avoid tension with Big Bang Nucleosynthesis [38]. However, for $m_V \sim$ few MeV, $V \to \nu\bar{\nu}$ decays after neutrino decoupling increase the neutrino/photon temperature ratio and yield $\Delta N_{\rm eff} \sim 0.2 - 0.5$, which can ameliorate the $\sim 3.5\sigma$ tension between cosmological and local measurements of the Hubble rate H_0 [23]; to the left of this band, $\Delta N_{\rm eff} > 0.5$, which is disfavored by CMB and BBN measurements under standard cosmological assumptions [30].

As shown in Fig. 1 (left panel), the asymptotic reach of $K \to \mu\nu X$ with X decaying invisibly could cover a large portion of the parameter space, far beyond the reach of present experiments. Conversely the reach of $K \to \mu\nu X$ with X decaying to di-muons is competitive with existing bounds from $BABAR$. The detailed study and the experimental challenges of the invisible and di-muon analysis are described in Sec. IV A and Sec. IV B respectively.

B. Adding $L_\mu - L_\tau$ Charged Dark Matter

If a light DM particle χ also couples to a new muonic force, the decay mode can significantly change the V branching fraction above the di-muon threshold; below this boundary, V always decays invisibly (either to neutrinos or DM). In this section we add a lighter ($m_V > 2m_\chi$) DM candidate χ charged under $L_\mu - L_\tau$ and extend Eq. (1) to include a coupling to the dark current $\mathcal{L} \supset g_\chi V_\mu J_\chi^\mu$. For representative DM candidates, we have

$$J_\chi^\mu = \begin{cases} i\chi^*\partial_\mu\chi + h.c. & \text{Complex Scalar} \\ \frac{1}{2}\overline{\chi}\gamma^\mu\gamma^5\chi & \text{Majorana} \\ \overline{\chi}\gamma^\mu\chi & \text{Dirac} \end{cases} \quad (3)$$

where $g_\chi \equiv g_V q_\chi$ is the total DM-V coupling and the DM's $L_\mu - L_\tau$ charge q_χ is a free parameter; throughout this paper we assume μ, τ and their neutrinos carry unit charge.

For $m_\chi < m_V$, freeze out proceeds via s-channel annihilation to SM final states and calculated abundance for each of the candidates in Eq. (3) can be found in [11, 39]. In the right panel of Fig. (1), we show representative targets for these DM candidates in the α_V vs. m_V plane alongside existing constraints on $L_\mu - L_\tau$ forces. Note that the $BABAR$ constraint from the left panel is absent because V decays predominantly to DM in this regime; future work will assess the B-factory reach for this scenario [33] (see also [40]). Note that the H_0 favored region
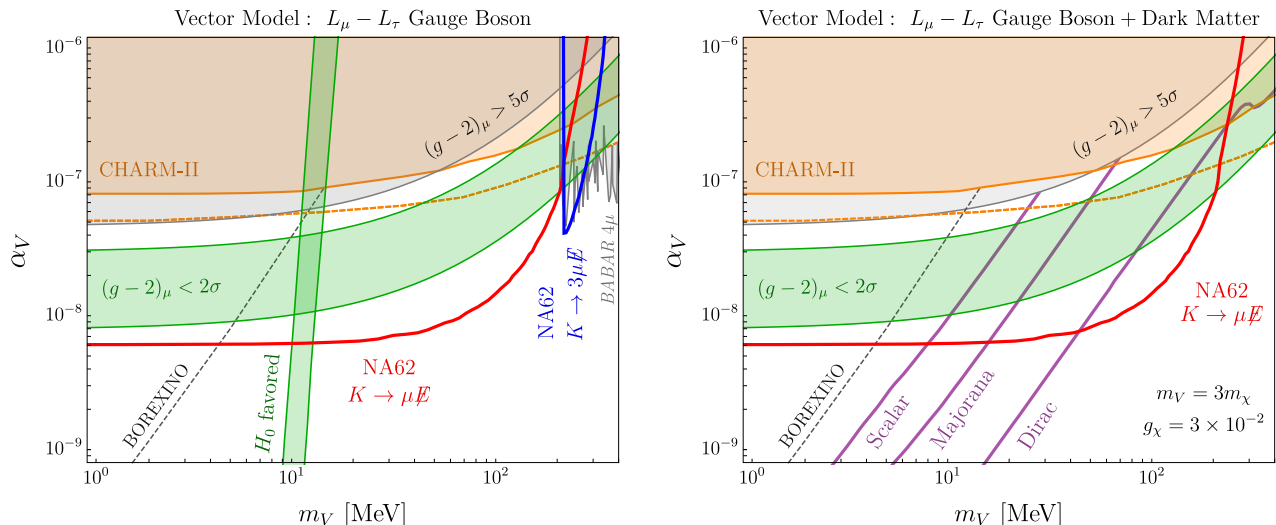
FIG. 1. **Left:** Parameter space for a gauged $L_\mu - L_\tau$ SM extension from Sec. II. $\alpha_V = g_V^2/4\pi$ where g_V is the coupling strength to the $\mu - \tau$ current. The light green band is the 2σ region accommodating the $(g-2)_\mu$ anomaly, while the dark green vertical region is the parameter space for which early universe $V \to \nu\bar\nu$ decays increase yield $\Delta N_{\rm eff} = 0.2 - 0.5$, ameliorating the $\sim 3.5\sigma$ tension between cosmological and local measurements of the Hubble rate H_0 [23]. We show projections for an NA62 search for $K^+ \to \mu^+\nu_\mu V$ followed by a prompt invisible $V \to \nu\bar\nu$ decay (red curve) or a prompt visible $V \to \mu^+\mu^-$ decay (blue curve). Both sensitivities assume the full NA62 luminosity to be recorded by the single muon and di-muon trigger respectively and systematic errors comparable to the statistical uncertainty (see Sec. IV and Appendix C for more details). The gray shaded regions are excluded by the *BABAR* 4μ search [25] and $(g-2)_\mu$. The shaded orange region is the CHARM-II μ-trident constraint [26, 27]; the dashed curve is the CCFR measurement [28] (see text for a discussion). **Right:** Same as left, only the V is now also coupled to a dark matter candidate χ, such that ${\rm BR}(V \to \chi\chi) \simeq 1$ over the full parameter space. Note that the H_0 band and the *BABAR* constraints no longer apply because V decays yield neither neutrinos (for H_0) nor muons (for *BABAR*). The purple bands represent the thermal freeze out parameter space for $\chi\chi$ annihilation to SM final states (neutrinos and muons, where kinematically allowed) through virtual s-channel V exchange. Note that for $m_\chi < m_\mu$ DM can only annihilate to neutrinos and hence is not subject to the BBN [29] or CMB [30] energy injection bounds on light DM.

is also absent because this band requires V to decay to neutrinos after decoupling.

III.   SCALAR FORCES

The minimal Lagrangian for a Yukawa muonic force is

$$\mathcal{L} = \frac{1}{2}(\partial_\mu \phi)^2 - \frac{m_\phi^2}{2}\phi^2 - y_\phi \phi \bar\mu\mu, \qquad (4)$$

where ϕ is a real scalar particle. The interaction in Eq. (4) can arise, for instance, by integrating out a heavy, vectorlike lepton singlets whose mass mixes with the right handed muon as discussed in Appendix B. In the absence of additional interactions, for $m_\phi > 2m_\mu$, the dominant decay is $\phi \to \mu^+\mu^-$ with partial width

$$\Gamma_{\phi\to\mu^+\mu^-} = \frac{\alpha_\phi m_\phi}{2}\left(1 - \frac{4m_\mu^2}{m_\phi^2}\right)^{3/2}, \qquad (5)$$

where $\alpha_\phi \equiv y_\phi^2/4\pi$. For $m_\phi < 2m_\mu$, the dominant channel is $\phi \to \gamma\gamma$ through a muon loop with width

$$\Gamma_{\phi\to\gamma\gamma} = \frac{\alpha_{\rm EM}^2 \alpha_\phi m_\phi^3}{64\pi^2 m_\mu^2}\left|\frac{2}{x^2}\left(x + (x-1)\arcsin^2\sqrt{x}\ \right)\right|^2, \qquad (6)$$

where $x \equiv m_\phi^2/4m_\mu^2$ and the lab frame decay length is

$$\ell_{\phi\to\gamma\gamma} \sim 60{\rm m}\left(\frac{3\times 10^{-6}}{\alpha_\phi}\right)\left(\frac{50\,{\rm MeV}}{m_\phi}\right)^4\left(\frac{E_\phi}{75\,{\rm GeV}}\right), \qquad (7)$$

where the m_ϕ^{-4} scaling accounts for the boost factor. In this minimal "visibly decaying" scenario, most of our favored parameter space is below the di-muon threshold, so the diphoton channel dominates and, for the maximum ϕ energy ~ 75 GeV, nearly all decays occur outside the NA62 detector to mimic a missing energy signature. However, a dedicated study is required to identify the distance beyond which these decays are invisible given NA62 kinematics and acceptance; we also note that it may be possible to perform a $\phi \to \gamma\gamma$ resonance search if this occurs inside the decay region.

Alternatively, ϕ may decay predominantly to undetected particles (e.g DM) in the "invisibly decaying" scenario. In both cases, the scalar is produced via $K \to \mu\nu\phi$ processes whose width is computed in Appendix A.

In Fig. 2 we present our NA62 projections for visible (left) and invisible (right) decays on the $\alpha_\phi \equiv y_\phi^2/4\pi$ vs. m_ϕ plane assuming 100% branching ratio in both channels. The main difference relative to the vector case is that the $K \to 3\mu\nu$ search improves considerably beyond the *BABAR* 4μ bounds; here the $e^+e^- \to \mu^+\mu^-\phi$
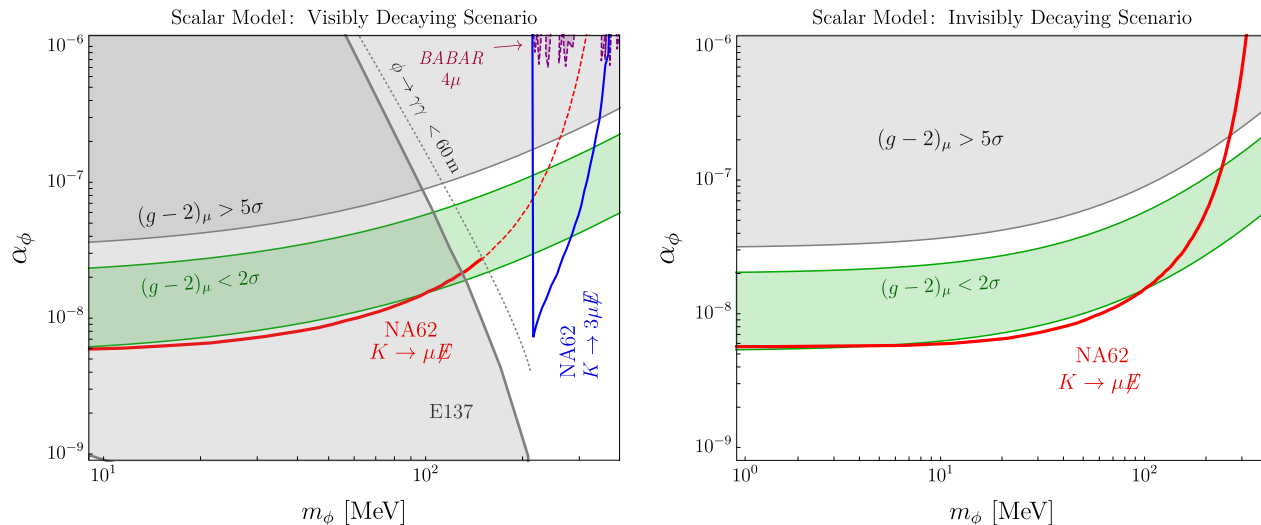
FIG. 2. Parameter space and NA62 projection for a muon-philic scalar particle ϕ described in Sec. III. Here we define $\alpha_\phi \equiv y_\phi^2/4\pi$ where y_ϕ is the Yukawa coupling to muons from Eq. (4) and the light green band is the 2σ region accommodating the $(g-2)_\mu$ anomaly. **Left:** Projections for an NA62 search for $K^+ \to \mu^+\nu_\mu\phi$ where ϕ decays visibly into $\phi \to \mu^+\mu^-$ or $\gamma\gamma$ where kinematically allowed. On the left of the dashed grey line the lifetime of the muon-philic scalar is long enough to give an invisible signal at NA62. Also shown are E137 constraints from [41]. **Right:** Same as the left, but here we assume that ϕ decays invisibly. Both sensitivities assume the full NA62 luminosity and the searches to be statistic dominated (see Sec. IV and Appendix C for more details). Note that in both panels for masses below an MeV, ϕ decays during BBN, so this parameter space is not shown.

cross section is much smaller for ϕ vs. V production. We also show the E137 bound for the visible decay scenario from [41] (see [42] for similar constraints). There are additional constraints from supernovae [41, 43] not included in the figure due to their large astrophysical uncertainties and significant model dependency in the invisible decaying scenario.

IV. RARE KAON DECAYS AT NA62

The electroweak coupling governing SM $K \to \mu\nu$ decays is

$$\mathcal{L} \supset (2G_F f_K V_{us}) \, \partial_\alpha K^- \bar{\nu}_\mu \gamma^\alpha P_L \mu + h.c., \qquad (8)$$

where G_F is the Fermi constant, $V_{us} = 0.223$ is the us CKM matrix element, and $f_K = 160$ MeV is the kaon decay constant. We are interested in three-body corrections to this process: $K^+ \to \mu^+\nu_\mu X$, where $X = V$ or ϕ, is emitted from a final state μ and/or ν_μ line. The differential decay distribution is

$$\frac{d\Gamma(K^+ \to \mu^+\nu X)}{dm_{\mathrm{miss}}^2} = \frac{1}{256\pi^3 m_K^3} \int \sum |\mathcal{M}|^2 dm_{\mu X}^2, \quad (9)$$

where $m_{\mu X}$ is the μX invariant mass while m_{miss}^2 is the missing invariant mass defined as

$$m_{\mathrm{miss}}^2 = (P_X + P_{\nu_\mu})^2 = (P_K - P_\mu)^2. \qquad (10)$$

The matrix element $|\mathcal{M}|^2$ is presented for both scalar and vector scenarios in Appendix A. Below we describe

two different search strategies depending on whether X decays invisibly or to muons.

A. Invisible analysis

If X is produced in $K^+ \to \mu^+\nu_\mu X$ events and decays *invisibly*, the m_{miss}^2 distribution $K \to \mu+$ invisible events differs from the SM prediction (see Appendix C for more details). The sensitivity of an m_{miss}^2 search in single muon events is computed using the log-likelihood ratio

$$\Lambda(S) = \sum_i -2\log \frac{L_i(S)}{L_i(\hat{S}=0)} \,, \qquad (11)$$

where L_i, the likelihood in each bin i, is constructed from a Poisson distribution,[3] and $S = N_{K^+}\,\mathcal{A}\,\mathrm{BR}(K^+ \to \mu^+\nu X)$ is the signal yield with acceptance $\mathcal{A} \simeq 0.35$. We require $\Lambda(S) < 4$ to define the 2σ sensitivity.

Our background sample is extracted from public NA62 data from the 2015 run in which 2.4×10^7 events passing the single muon trigger were recorded [44]. These data yield $N_{K^+} \approx 10^8$ kaons after dividing out the detector acceptance and SM branching ratio $\mathrm{BR}(K^+ \to \mu^+\nu_\mu) =$

––––––––

[3] $L_i(S) = \frac{(S\epsilon_{Si}+B_i)^{D_i}}{D_i!}e^{-(S\epsilon_{Si}+B_i)}$ where D_i, B_i, and ϵ_{Si} are data, background, and signal fraction in each bin. The maximum likelihood estimator is $\hat{S} = 0$ under the assumptions behind our projections, $D_i = B_i$.

0.63; all events in this sample are binned in missing mass intervals of 4×10^{-3} GeV^2.

One of the main backgrounds for this search is $K \to \mu\nu(\gamma)$, in which a radiated γ is not detected and contributes to the missing energy. This process peaks at $m^2_{\mathrm{miss}} = 0$ and its contribution to the large missing mass tail depends NA62's photon rejection efficiency. Due to this large background, including missing mass bins below $m^2_{\mathrm{miss}} = 2.3 \times 10^{-2}$ GeV^2 does not change the log-likelihood ratio defined in Eq. (11).

In the 2015 data sample, other backgrounds are present at large m^2_{miss} and exceed the $K \to \mu\nu(\gamma)$ tail for $m^2_{\mathrm{miss}} > 0.1$ GeV^2. These events are largely due to the muon halo and we expect their contribution to be substantially reduced in the 2017 dataset where NA62 utilizes a silicon pixel detector (GTK) to measure the timing and momentum of upstream Kaons [22]. To approximately account for this existing improvement, we rescale the background yield above $m^2_{\mathrm{miss}} > 2.3 \times 10^{-2}$ GeV^2 by an additional factor of four to estimate our sensitivity.[4]

Maximizing signal sensitivity is challenging for two main experimental reasons:

1. **Single muon trigger bandwidth:** This issue is related to the large number of single muon events arising from SM $K \to \mu\nu$ decays. Thus, the current single muon trigger at NA62 is rescaled by $1/400$ [45], so only one single muon event out of 400 is recorded, which reduces the sensitivity of our search. This limitation can be overcome with a dedicated single muon trigger with a lower cut on the missing mass at trigger level (or equivalently an upper cut on the muon momentum). In the 2015 data sample, despite over 2.4×10^7 events passing the single muon trigger, only 5.6×10^3 have $m^2_{\mathrm{miss}} > 2.3 \times 10^{-2}$ GeV^2. Thus, with a dedicated trigger, it would be possible to record *all* events with $m^2_{\mathrm{miss}} > 2.3 \times 10^{-2}$ GeV^2 and keep the $1/400$ trigger rescaling for those with lower m_{miss}. Our search strategy exploits this possibility and utilizes the full NA62 luminosity $N_{K^+} \approx 10^{13}$ in the decay region, which we assume for our projections.

2. **Background systematics for large m^2_{miss}:** Unfortunately these systematics are difficult to estimate from the 2015 data release in which there is disagreement between data and Monte Carlo (MC) modeling at large m_{miss}. A careful experimental effort is required to assess these uncertainties. Since our goal here is to show how much the sensitivity of NA62 could be improved under the most optimistic circumstances, our analysis presents results with only statistical errors; these can only be achieved once systematic uncertainties become subdominant

for the full NA62 luminosity: $\sigma_{\mathrm{sys}}/B < B^{-1/2} \sim 10^{-4}$. In Figs. II and III we present future sensitivities assuming systematics are negligible, but note that exploring new parameter space in this plane only requires systematic uncertainties to be below 1%. In Appendix C 1 we show how our results vary under different assumptions regarding systematic errors.

B. Di-muon analysis

If X is produced in $K^+ \to \mu^+\nu_\mu X$ events and decays *visibly* to di-muons, NA62 can improve upon previous experiments in the $K^+ \to 2\mu^+\mu^-\nu$ channel. The SM prediction for this branching ratio is BR($K^+ \to 2\mu^+\mu^-\nu)_{\mathrm{SM}} = 1.3 \times 10^{-8}$ [46] and currently has not been observed experimentally; the best limit on this process comes from the E787 measurement BR($K^+ \to 2\mu^+\mu^-\nu)_{\mathrm{obs}} < 4.1 \times 10^{-7}$ in 1989 [24]. With the present luminosity ($\sim 10^{11} K^+$ [45]), NA62 should already have recorded at least 100 such events passing the di-muon trigger. Here we propose a di-muon resonance search in $K^+ \to \mu^+\nu X(\mu^+\mu^-)$ events with opposite sign (OS) di-muon pairs.

Since these data have not been released by the NA62 collaboration yet, we estimate the sensitivity of the search from our MC simulation. We implement the effective weak interaction of Eq. (8), the electromagnetic interactions of K^+ decays, and the new physics couplings from Eqs. (1) and (4) in MadGraph 5 v2 LO [47, 48]. Both the background and the signal in $2\mu^+\mu^-\nu$ final state are simulated. In Figs 1 (left) and 2 (left) we present the results of this analysis in blue curves labeled NA62 $K \to 3\mu\slashed{E}$. Systematic uncertainties on the background will affect less the result compared to the invisible channel because a data-driven background estimate would be possible. For more details about our projection, see Appendix C 2.

V. CONCLUSION

In this letter we have shown that rare kaon decay searches at NA62 can probe most of the remaining parameter space for which muonic-philic particles resolve the $\sim 3.5\sigma$ $(g-2)_\mu$ anomaly; these are the only viable explanations involving particles below the weak scale. The same parameter space can also accommodate thermal DM production or reduce the H_0 tension if the new particle decays to DM or neutrinos, respectively.

If this new particle decays invisibly, achieving this sensitivity requires a dedicated single muon trigger to record all $K^+ \to \mu^+ +$invisble events with $m^2_{\mathrm{miss}} > 0.05$ GeV^2 during Run 3. The ultimate reach in this channel depends crucially on the systematic uncertainties on events with these kinematics; a dedicated experimental study is needed to assess the feasibility of this requirement.

---

[4] We thank Evgueni Goudzovski and Babette Döbrich for discussions on this.

If the new particle decays visibly to di-muons, we find that NA62 can improve existing bounds with a resonance search in opposite sign muons in $K^+ \to 2\mu^+\mu^-\nu_\mu$ events. The improvement is marginal if the muonic force is mediated by a vector but substantial in the scalar case. This proposed search is based on already existing trigger and can be performed on the data already recorded during Run 2.

Finally, we note that if the $(g-2)_\mu$ anomaly is confirmed, NA62 can play important role in deciphering the new physics responsible for the discrepancy. However, even if future measurements are consistent with the SM, the searches we propose can still explore parameter space for which muonic forces mediate dark matter production via thermal freeze out. Such measurements can also inform future decisions about proposed dedicated experiments including NA64μ[19], M^3[11], BDX [49, 50], and LDMX [51, 52].

Appendix A: Decay Calculation

The SM width $K \to \mu\nu$ can be written as

$$\Gamma(K^+ \to \mu^+\nu) = \frac{m_K \lambda_\mu^2}{2\pi}\left(1 - \frac{m_\mu^2}{m_K^2}\right)^2 . \qquad (A.1)$$

where the coupling

$$\lambda_\mu \equiv 2G_F f_K m_\mu V_{us} \simeq 8.7 \times 10^{-8}, \qquad (A.2)$$

sets the typical size of the kaon decay widths considered here. Note that λ_μ has to be proportional to the muon mass because a chirality flip is required to make the amplitude non-zero. The kaon width is $\Gamma_{K^+} = 5.3 \times 10^{-14}$ MeV, so $\text{BR}_{K\to\mu\nu} \simeq 0.63$. Below we present the calculation for the squared matrix elements of

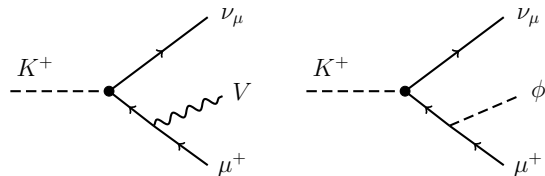$$K^+(P) \to \mu^+(k)\nu_\mu(q)X(\ell) , \qquad (A.3)$$

FIG. 3. Two representative Feynman diagrams that contribute to rare kaon decays involving a light, invisibly decaying vector from Sec. II (left) and scalar from Sec. III (right). In the vector case there is another diagram where the vector radiates off from the neutrino line. This is not shown but it is included in our result.

where $X = V$ or ϕ is a muonic force carrier considered in this paper and P, k, q and ℓ are four vectors. These results are already present in the extensive literature on muonic forces (see for example [53]) but we present them here for completeness.

For either scenario, the partial width for this process can be written as

$$\Gamma_{K\to\mu\nu_\mu X} = \frac{1}{256\pi^3 m_K^3}\int\sum|\mathcal{M}_X|^2 dm_{12}^2 dm_{23}^2 , \quad (A.4)$$

where the limits of integration are given by $(m_{12}^2)_{\min} = m_X^2$ and $(m_{12}^2)_{\max} = (m_K - m_\mu)^2$. For a fixed m_{12} the minimum and maximum of m_{23} are given by

$$(m_{23}^2)_{\max}^{\min} = (E_2^* + E_3^*)^2 - \left(\sqrt{E_2^{*2} - m_X^2} \pm \sqrt{E_3^{*2} - m_\mu^2}\right)^2, \quad (A.5)$$

where we define

$$E_2^* = \frac{m_{12}^2 + m_X^2}{2m_{12}} , \quad E_3^* = \frac{m_K^2 - m_{12}^2 - m_\mu^2}{2m_{12}} . \quad (A.6)$$

In Fig. 4 we plot for completeness the normalized signal rates for both the vector and the scalar model.

1. Vector Mediator

For the vector model introduced in Sec. II with $X = V$, our process of interest arises from the Feynman diagram in Fig. 3 and also contains an additional diagram with V emitted from the ν_μ. The squared matrix element is

$$|\mathcal{M}_V|^2 = g_V^2 \lambda_\mu^2\left[2 + \frac{(m_{12}^2 + 2m_\mu^2 - 2m_K^2)}{m_{23}^2 - m_\mu^2}\right.$$
$$-\frac{(m_K^2 - m_\mu^2)(m_V^2 + 2m_\mu^2)}{(m_{23}^2 - m_\mu^2)^2} + 2\frac{(m_K^2 - m_\mu^2)^2 + m_V^2 m_\mu^2}{m_{12}^2(m_{23}^2 - m_\mu^2)}$$
$$\left.-\frac{m_V^2(m_K^2 - m_\mu^2)}{m_{12}^4} + \frac{(m_{23}^2 + m_\mu^2 - 2m_K^2)}{m_{12}^2}\right], \qquad (A.7)$$

where $k\,q$ and l are respectively the μ, ν and V momenta and we define $m_{12} = (\ell + q)^2$ and $m_{23} = (\ell + k)^2$. Note that the full matrix element vanishes for $m_\mu \to 0$ due to chiral symmetry.
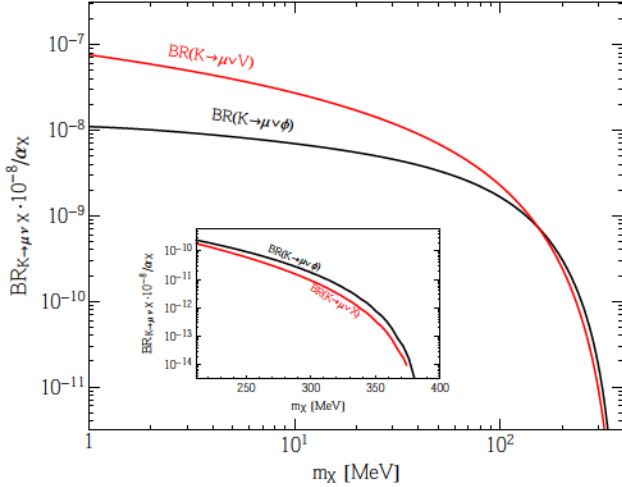
FIG. 4. Total branching ratio for $K \to \mu\nu X$ where X is a vector V (red) or a scalar ϕ (black) as a function of the the mass of X. In the small quadrant we give a zoom of the relevant region for $K \to \mu\nu X(2\mu)$.

2. Scalar Mediator

For the muon-philic scalar introduced in Sec. III, the squared matrix element is

$$|\mathcal{M}|^2 = \frac{\lambda_\mu^2 y_\phi^2}{2m_\mu^2(m_{23}^2 - m_\mu^2)^2}\left[m_K^2(m_{23}^2 + m_\mu^2)^2 \right.$$
$$-m_{23}^2\left((m_{23}^2 + m_\mu^2)^2 + m_{12}^2(m_{23}^2 - m_\mu^2)\right)$$
$$\left. +m_\phi^2(m_{23}^2 - m_\mu^2 m_K^2)\right], \qquad (A.8)$$

where m_{23} is defined below Eq. (A.7). The squared matrix element above does vanish for $m_\mu \to 0$ because the scalar yukawa interactions with the muons in Eq. 4 breaks the chiral symmetry independently of the muon mass.

Appendix B: Complete Scalar Model

Before electroweak symmetry breaking, the Yukawa interaction in Eq. (4) is forbidden by gauge symmetry. The simplest gauge invariant operator that gives rise to this Yukawa interaction is the dimension 5 operator

$$\phi L H \mu^c, \qquad (B.1)$$

where L is the second generation lepton doublet and μ^c the muon singlet in 2-component spinor notation.

In this Appendix we present a UV completion of the model which gives rise to this interactions after integrating out heavy fermionic degrees of freedom (see e.g. [13, 54, 55] for other alternatives). This construction differs from the ones in [20] in that the coupling to muons does not arise due to the scalar mixing with the Higgs. In particular the Higgs-scalar mixing is loop suppressed in this model and can be parametrically smaller in a technically natural manner; thus, as discussed below, many of the scalar bounds presented in [13] do not apply for an equivalent $\phi - \mu$ coupling.

The model includes an extra vector-like pair of fermions in which one of these carries the same gauge quantum numbers as μ^c and the other carries compensating quantum numbers to cancel anomalies. This extension can generate the required coupling through mixing between this new fermion and the muon. The relevant terms in the Lagrangian of the model are

$$\mathcal{L} \supset y_\mu L H \mu^c + M\psi\psi^c + \lambda_1\phi\psi\psi^c + \lambda_2\phi\psi\mu^c$$
$$+ y_\psi L H \psi^c + h.c., \qquad (B.2)$$

where (ψ, ψ^c) is the new vector like fermion pair. Note that we chose to not include a mass mixing term $\mu^c\psi$ which is allowed by all the symmetries, since this term can be removed by an appropriate field redefinition.

Assuming $M > v$, we can integrate out the new fields before electroweak symmetry breaking. This generates the following new terms

$$-\lambda_2 y_\psi \frac{\phi}{M} L H \mu^c + \frac{\lambda_1\alpha}{6\pi M}\phi F^{\mu\nu}F_{\mu\nu}, \qquad (B.3)$$

where F is the photon field strength. After electroweak symmetry breaking the first term in the above interaction generates the coupling in Eq. (4), with

$$y_\phi = -\frac{\lambda_2 y_\psi v}{\sqrt{2}M}. \qquad (B.4)$$

The second term in Eq. (B.3) contributes to the scalar decay to photons. Depending on the choice of parameters the contribution from this term can be larger than the IR contribution from the muon loop and the partial width to photons in Eq. (6) must be corrected. This shows that different choice of UV parameters can lead to either prompt or displaced decays to photons, which highlights the complementarity of performing both an invisible search and a diphoton resonance search.

The couplings in Eq. (B.2) induce a ϕ-Higgs mixing at loop level. We can estimate the size of the mixing from the contributions involving λ_1 and λ_2 to be

$$\frac{\lambda_1 y_\psi^2}{16\pi^2}Mv\phi h, \qquad \frac{\lambda_2 y_\psi^2}{16\pi^2}Mv\phi h. \qquad (B.5)$$

This induces mixing angles much smaller than the $\sim 10^{-3}$ bound discussed in [13, 56] for all of the parameter space we are interested in. One can also easily show that the decay to electrons induced by the mixing with the Higgs is small compared to the diphoton decay from the ϕF^2 coupling.

Appendix C: NA62 Analysis

Here we provide additional details about the procedure with which NA62 projections are computed this paper.
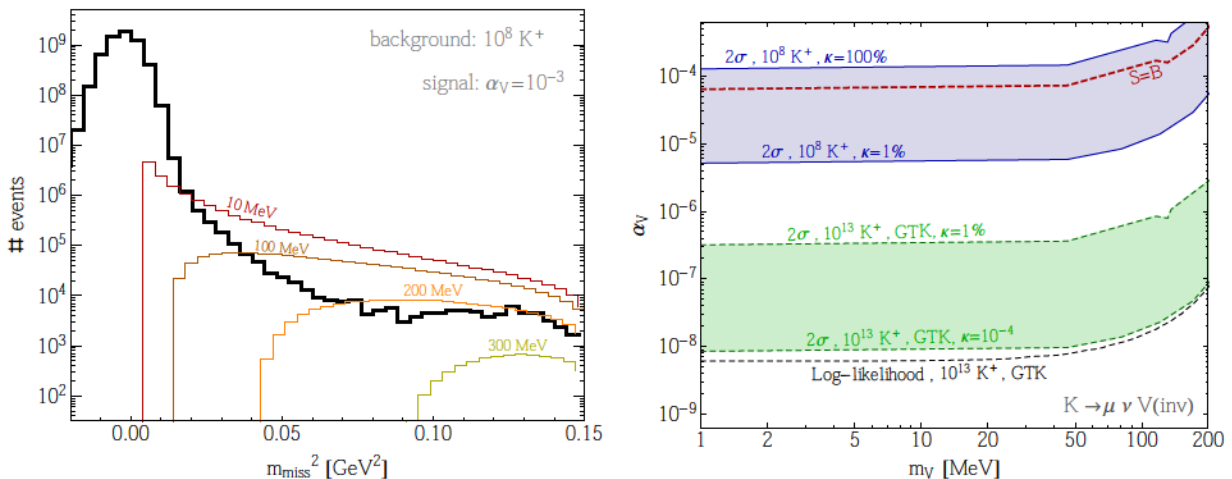
FIG. 5. **Left:** Missing invariant mass distribution for $K \to \mu\nu V$ decays for different masses of V (in different colors) where m_{miss}^2 is the combined invariant mass of V and ν_μ in Eq. (9). The missing mass distribution is very similar. In the scalar case very similar distributions are obtained. The black line correspond to the background distribution extracted from [44]. The data are binned in squared invariant mass bins of 4×10^{-3} GeV^2. **Right:** Sensitivity at 2σ level of the invisible search for modification of the missing mass tail from $K \to \mu\nu V (V \to \text{invisible})$. The red dashed line shows when the signal is equal to the background extracted from the 2015 data after applying the missing mass cut. The blue band is the present sensitivity based on 10^8 kaons collected in 2015; the thickness of the band encompasses different assumptions about the magnitude of background systematic uncertainties. The green band shows the future sensitivity based on 10^{13} kaons with different systematics. A background suppression at large missing mass is assumed to account for the GTK installation. The dashed black line is based on the likelihood analysis described in Sec. IV A, here the background uncertainty is assumed to be dominated by statistics.

In particular, we present the background distributions for both the visible and invisible analyses and comment on how different assumptions regarding systematic errors affect these projections.

1. Invisible analysis

In Fig. 5 left we compare the m_{miss}^2 distribution for $K \to \mu\nu X$ signal events for different X masses using the background shape extracted from NA62 public data [44]. The signal here is shown for $X = V$ but the scalar case is qualitatively similar. Note that the signal reduction at small m_{miss}^2 is m_X dependent, so an optimal m_{miss} can be chosen for different values to maximize sensitivity. As discussed in Sec. IV A, the background at large missing mass does not appear to scale as one might expect if it were dominated by the QED radiative tail from $K \to \mu\nu(\gamma)$ decays. The reason is that other backgrounds including the halo muon background and $K \to 3\pi$ become dominant in this regime. We believe that these backgrounds will be further suppressed in future data releases for which timing and momentum of the kaon will be measured upstream with the silicon pixel detector (GTK), which has already been used for the 2017 run. To roughly account for this improvement, we rescale the background above $m_{\text{miss}}^2 > 0.023$ GeV^2 by an additional factor of four.

In Fig. 5 right we show estimated 2σ sensitivities for the vector case computed in a cut-and-count experiment;

similar results are also found for the scalar case. This simpler analysis is performed here and compared to the likelihood analysis presented in the main text in order to quantitatively show the effects of systematic uncertainties on the background.

The 2σ sensitivity of an m_{miss}^2 search in single muon events is computed by evaluating $S/\sqrt{B + \kappa^2 B^2} = 2$, where the S is the number signal events, B the number of background events and $\kappa = \sigma_{\text{sys}}/B$ is the systematic uncertainty on the background. The signal yield is

$$S = \frac{N_{K^+} \mathcal{A}}{\Gamma_{K^+}} \int_{m_{\text{cut}}^2}^{m_{\text{max}}^2} dm_{\text{miss}}^2 \frac{d\Gamma_{K^+ \to \mu^+\nu X}}{dm_{\text{miss}}^2}, \quad \text{(C.1)}$$

where $\mathcal{A} \simeq 0.35$ is the the detector acceptance. m_{cut} is the lower cut on the missing mass, which is optimized for each value of m_X to maximize signal sensitivity, but always satisfies $m_{\text{cut}}^2 > 0.05$ GeV^2; $m_{\text{max}}^2 = (m_K - m_\mu)^2 = 0.15$ GeV^2 is the maximum kinematically allowed missing mass.[5]

From Fig. 5 it is clear that the future NA62 sensitivity depends greatly on background systematics at large

---

[5] Note that $m_{\text{cut}}^2 = 0.05$ GeV^2 is the *minimal* missing mass cut in our cut and count analysis. This should not be confused with $m_{\text{miss}}^2 = 0.023$ GeV^2 which is the value of the invariant mass below which adding bins to the log-likelihood ratio in Eq. (11) does not effectively improve signal sensitivity. Of course the physics behind these two quantities is very similar and related to the background shape peaking at $m_{\text{miss}} = 0$.
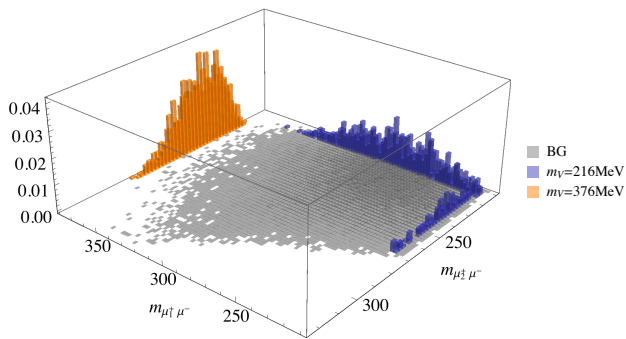
FIG. 6. Normalized 2D distributions of $m_{\mu_1^+\mu^-}$ and $m_{\mu_2^+\mu^-}$ for signal of two benchmark points ($m_V = 216, 376$ MeV) and the SM background. The muon momenta are evaluated in the K^+ rest frame, and μ_1^+ corresponds to the leading muon and μ_2^+ is the other. As expected, μ_1^+ leads to a peak of $V(\phi)$ for the higher mass of the muonic force, while μ_2^+ does the same for the lower mass.

missing mass. For the present/future luminosity, the blue/green lines at the bottom of these bands correspond to systematic uncertainty $\kappa_{\min}$ for which the statistical uncertainty becomes dominant. This can be estimated as a function of the luminosity and the number of background events for a given missing mass cut

$$\kappa_{\min} \simeq \frac{1}{\sqrt{B}} \simeq (4 \times 10^{-2}, 2.5 \times 10^{-4}), \qquad \text{(C.2)}$$

where the first number assumes 10^8 kaons and 652 background events after a missing mass cut of $m_{\text{miss}}^2 > 0.05$ GeV^2 and the second number assumes 10^{13} kaons and 1.6×10^7 background events (accounting for the expected background suppression). For comparison we also show in Fig. 5 the most aggressive reach derived from our likelihood analysis. As expected, the log-likelihood improves the reach for low mass resonances where the signal spreads widely in the large background region (see Fig. 5 left) and a simple cut-and-count analysis poorly distinguishes the signal from background.

2. Di-muon analysis

In this section we describe the proposed opposite-sign di-muon resonance analysis in $K \to 3\mu\nu$ events, which defines the blue projections in Fig. 1 (left) and 2 (left) labeled NA62 $K \to 3\mu + \not{E}$. We assume that the irreducible SM background for our search arises from K^+ decays to three muons through an off-shell gauge boson and neglect other possible backgrounds from non-detection of photons, $\pi^\pm$ misidentification and decay which are expected to be in the same order or subdominant. Moreover, for simplicity, we assume acceptance for both signal and background to be 5%. This number is roughly 1/6 of the acceptance reported in [44] for the single muon trigger and should roughly account for the extra cost of requiring three muons to pass trigger and identification criteria.

The other challenge of this search is the ambiguity in choosing the opposite-sign di-muon pair to reconstruct the X invariant mass. To resolve this problem we choose the opposite-sign di-muon pair that gives an invariant mass closer to each test mass for the signal. Typically it is the leading muon above $m_X \simeq 300$ MeV, and the second leading one below $m_X \simeq 260$ MeV as seen in Fig. 6. After this choice is made, we select the signal and the background within a narrow invariant mass bin around each test mass $[m_X - 2\delta m_{\mu^+\mu^-}, m_X + 2\delta m_{\mu^+\mu^-}]$. The invariant mass bin size can be determined as a function of the smearing of the muon momentum in the NA62 detector

$$\frac{\delta m_{\mu^+\mu^-}}{m_X} = \frac{1}{2}\left(\frac{\delta p_{\mu_+}}{p_{\mu_+}} \oplus \frac{\delta p_{\mu_-}}{p_{\mu_-}}\right) \qquad \text{(C.3)}$$

where δp_μ is the muon momentum resolution of the NA62 detector, which satisfies [44]

$$\frac{\delta p_\mu}{p_\mu} = 0.3\% \oplus \left(0.005 \, \frac{p_\mu}{\text{GeV}}\right), \qquad \text{(C.4)}$$

where $\oplus$ indicates a sum in quadrature. The muon momentum is fixed to be $p_{\mu_\pm} = 20$ GeV($\sim p_{K^+}/4$). The future sensitivities of this search at 2σ in Fig 1 left and in Fig 2 assume 10^{13} kaons and uncertainties dominated by statistics. Systematic uncertainties on the background can be under control because the data-driven background estimate (side-band) is made possible by the peaked nature of the signal.

[1] R. Essig *et al.*, in *Proceedings Snowmass on the Mississippi (CSS2013): Minneapolis, MN, USA, July 29-August 6, 2013* (2013) arXiv:1311.0029 [hep-ph].
[2] M. Battaglieri *et al.*, (2017), arXiv:1707.04591 [hep-ph].
[3] J. Alexander *et al.* (2016) arXiv:1608.08632 [hep-ph].
[4] G. W. Bennett *et al.* (Muon g-2), Phys. Rev. **D73**, 072003 (2006), arXiv:hep-ex/0602035 [hep-ex].
[5] K. Hagiwara, R. Liao, A. D. Martin, D. Nomura, and T. Teubner, J. Phys. **G38**, 085003 (2011), arXiv:1105.3149 [hep-ph].
[6] M. Davier, A. Hoecker, B. Malaescu, and Z. Zhang, Eur. Phys. J. **C71**, 1515 (2011), [Erratum: Eur. Phys. J.C72,1874(2012)], arXiv:1010.4180 [hep-ph].
[7] M. Pospelov, Phys. Rev. **D80**, 095002 (2009), arXiv:0811.1030 [hep-ph].
[8] G. Mohlabeng, (2019), arXiv:1902.05075 [hep-ph].

[9] G. Bertone and D. Hooper, Rev. Mod. Phys. **90**, 045002 (2018), arXiv:1605.04909 [astro-ph.CO].

[10] P. Agrawal, Z. Chacko, and C. B. Verhaaren, JHEP **08**, 147 (2014), arXiv:1402.7369 [hep-ph].

[11] Y. Kahn, G. Krnjaic, N. Tran, and A. Whitbeck, JHEP **09**, 153 (2018), arXiv:1804.03144 [hep-ph].

[12] M. Reece and L.-T. Wang, JHEP **07**, 051 (2009), arXiv:0904.1743 [hep-ph].

[13] B. Batell, N. Lange, D. McKeen, M. Pospelov, and A. Ritz, Phys. Rev. **D95**, 075003 (2017), arXiv:1606.04943 [hep-ph].

[14] M. Ibe, W. Nakano, and M. Suzuki, Phys. Rev. **D95**, 055022 (2017), arXiv:1611.08460 [hep-ph].

[15] S. Martellotti, in *Proceedings, 12th Conference on the Intersections of Particle and Nuclear Physics (CIPANP 2015): Vail, Colorado, USA, May 19-24, 2015* (2015) arXiv:1510.00172 [physics.ins-det].

[16] J. Grange *et al.* (Muon g-2), (2015), arXiv:1501.06858 [physics.ins-det].

[17] T. M. and, Chinese Physics C **34**, 745 (2010).

[18] P. Abbon *et al.* (COMPASS), Nucl. Instrum. Meth. **A577**, 455 (2007), arXiv:hep-ex/0703049 [hep-ex].

[19] S. N. Gninenko, N. V. Krasnikov, and V. A. Matveev, Phys. Rev. **D91**, 095015 (2015), arXiv:1412.1400 [hep-ph].

[20] C.-Y. Chen, M. Pospelov, and Y.-M. Zhong, Phys. Rev. **D95**, 115005 (2017), arXiv:1701.07437 [hep-ph].

[21] Y. Kaneta and T. Shimomura, PTEP **2017**, 053B04 (2017), arXiv:1701.00156 [hep-ph].

[22] N. Collaboration, .

[23] M. Escudero, D. Hooper, G. Krnjaic, and M. Pierre, (2019), arXiv:1901.02010 [hep-ph].

[24] M. S. Atiya *et al.*, Phys. Rev. Lett. **63**, 2177 (1989).

[25] J. P. Lees *et al.* (BaBar), Phys. Rev. **D94**, 011102 (2016), arXiv:1606.03501 [hep-ex].

[26] D. Geiregat *et al.* (CHARM-II), Phys. Lett. **B245**, 271 (1990).

[27] W. Altmannshofer, S. Gori, M. Pospelov, and I. Yavin, Phys. Rev. Lett. **113**, 091801 (2014), arXiv:1406.2332 [hep-ph].

[28] S. R. Mishra *et al.* (CCFR), Phys. Rev. Lett. **66**, 3117 (1991).

[29] P. F. Depta, M. Hufnagel, K. Schmidt-Hoberg, and S. Wild, (2019), arXiv:1901.06944 [hep-ph].

[30] N. Aghanim *et al.* (Planck), (2018), arXiv:1807.06209 [astro-ph.CO].

[31] X.-G. He, G. C. Joshi, H. Lew, and R. R. Volkas, Phys. Rev. **D44**, 2118 (1991).

[32] T. Adams *et al.* (NuTeV), Phys. Rev. **D61**, 092001 (2000), arXiv:hep-ex/9909041 [hep-ex].

[33] G. Krnjaic, G. Marques-Tavares, D. Redigolo, and K. Tobioka, *In Preparation.*

[34] G. Bellini *et al.*, Phys. Rev. Lett. **107**, 141302 (2011), arXiv:1104.1816 [hep-ex].

[35] R. Harnik, J. Kopp, and P. A. N. Machado, JCAP **1207**, 026 (2012), arXiv:1202.6073 [hep-ph].

[36] M. Bauer, P. Foldenauer, and J. Jaeckel, JHEP **07**, 094 (2018), arXiv:1803.05466 [hep-ph].

[37] H. K. Dreiner, J.-F. Fortin, J. Isern, and L. Ubaldi, Phys. Rev. **D88**, 043517 (2013), arXiv:1303.7232 [hep-ph].

[38] M. Pospelov and J. Pradler, Ann. Rev. Nucl. Part. Sci. **60**, 539 (2010), arXiv:1011.1054 [hep-ph].

[39] A. Berlin, D. Hooper, G. Krnjaic, and S. D. McDermott, Phys. Rev. Lett. **121**, 011102 (2018), arXiv:1803.02804 [hep-ph].

[40] T. Araki, S. Hoshino, T. Ota, J. Sato, and T. Shimomura, Phys. Rev. **D95**, 055006 (2017), arXiv:1702.01497 [hep-ph].

[41] L. Marsicano, M. Battaglieri, A. Celentano, R. De Vita, and Y.-M. Zhong, Phys. Rev. **D98**, 115022 (2018), arXiv:1812.03829 [hep-ex].

[42] M. J. Dolan, T. Ferber, C. Hearty, F. Kahlhoefer, and K. Schmidt-Hoberg, JHEP **12**, 094 (2017), arXiv:1709.00009 [hep-ph].

[43] C.-Y. Chen, J. Kozaczuk, and Y.-M. Zhong, JHEP **10**, 154 (2018), arXiv:1807.03790 [hep-ph].

[44] E. Cortina Gil *et al.* (NA62), Phys. Lett. **B778**, 137 (2018), arXiv:1712.00297 [hep-ex].

[45] E. Cortina Gil *et al.* (NA62), (2018), arXiv:1811.08508 [hep-ex].

[46] J. Bijnens, G. Ecker, and J. Gasser, Nucl. Phys. **B396**, 81 (1993), arXiv:hep-ph/9209261 [hep-ph].

[47] J. Alwall, M. Herquet, F. Maltoni, O. Mattelaer, and T. Stelzer, JHEP **06**, 128 (2011), arXiv:1106.0522 [hep-ph].

[48] J. Alwall, R. Frederix, S. Frixione, V. Hirschi, F. Maltoni, O. Mattelaer, H. S. Shao, T. Stelzer, P. Torrielli, and M. Zaro, JHEP **07**, 079 (2014), arXiv:1405.0301 [hep-ph].

[49] M. Battaglieri *et al.* (BDX), (2017), arXiv:1712.01518 [physics.ins-det].

[50] M. Battaglieri *et al.* (BDX), (2016), arXiv:1607.01390 [hep-ex].

[51] A. Berlin, N. Blinov, G. Krnjaic, P. Schuster, and N. Toro, (2018), arXiv:1807.01730 [hep-ph].

[52] T. kesson *et al.* (LDMX), (2018), arXiv:1808.05219 [hep-ex].

[53] C. E. Carlson and B. C. Rislow, Phys. Rev. **D86**, 035013 (2012), arXiv:1206.3587 [hep-ph].

[54] C.-Y. Chen, H. Davoudiasl, W. J. Marciano, and C. Zhang, Phys. Rev. **D93**, 035006 (2016), arXiv:1511.04715 [hep-ph].

[55] B. Batell, A. Freitas, A. Ismail, and D. Mckeen, Phys. Rev. **D98**, 055026 (2018), arXiv:1712.10022 [hep-ph].

[56] G. Krnjaic, Phys. Rev. **D94**, 073009 (2016), arXiv:1512.04119 [hep-ph].